

PAPER • OPEN ACCESS

In-flight sensing of pollen grains via laser scattering and deep learning

To cite this article: James A Grant-Jacob *et al* 2021 *Eng. Res. Express* **3** 025021

View the [article online](#) for updates and enhancements.



PAPER

In-flight sensing of pollen grains via laser scattering and deep learning

OPEN ACCESS

RECEIVED

22 January 2021

REVISED

29 April 2021

ACCEPTED FOR PUBLICATION

4 May 2021

PUBLISHED

12 May 2021

Original content from this work may be used under the terms of the [Creative Commons Attribution 4.0 licence](#).

Any further distribution of this work must maintain attribution to the author(s) and the title of the work, journal citation and DOI.



James A Grant-Jacob , Matthew Praeger , Robert W Eason and Ben Mills

Optoelectronics Research Centre, University of Southampton, Southampton, SO17 1BJ, United Kingdom

E-mail: J.A.Grant-Jacob@soton.ac.uk**Keywords:** Deep learning, Imaging, Sensing, Optics, Pollen, Hay fever**Abstract**

The identification and imaging of pollen grains in-flight was performed via illumination of the pollen grains with three collinear laser beams that had central wavelengths of 450 nm, 520 nm and 635 nm. Two neural networks are reported here; the first neural network was able to categorise pollen grain species from their scattering patterns with ~86% accuracy, while the second neural network generated images of the pollen grains from their scattering patterns. This work demonstrates the potential application of laser scattering and deep learning for real-world in-flight pollen identification.

Introduction

In the UK, more than 10 million people suffer from hay fever [1], with the susceptibility of sufferers varying depending on the types of pollen, such as weed or grass pollen [2, 3]. Hay fever symptoms include sinusitis, nasal polyposis, conjunctivitis, otitis media with effusion, upper respiratory infections and sleep disorders [4–6]. Since some people may be more susceptible to specific types of pollen, it is therefore important to determine the type and number of individual species in a person's vicinity, as this may provide diagnostic information for their allergy. In addition, monitoring of pollen grains could provide greater information regarding pollen distribution for tracking of seasonal levels [7–9], regional and worldwide levels [10–13], and linking these to health effects [14]. Furthermore, this information could benefit studies on transport of pollen, such as from one country to another [15], insect migrations [16], as well as forecasting for crop production [17]. Current routine techniques for determining airborne particulate matter involve large filter gathering systems, such as Burkard traps [18–20], which can then enable microscopy and chemical identification in a specialised laboratory.

Recently explored methods for faster identification of individual pollen grains include an automated microscope to identify pollen grains [21] and deep learning methods for the classification of pollen grain species from their visible light microscope images [22–27]. The need for increased temporal and spatial resolution of pollen distribution has led to research into real-time monitoring of aerosols, and specifically pollen [28], that include using robotic systems with [29] and without deep learning for pollen classification [30, 31], as well as optical particle counters that use the scattering of light to detect pollen [32–34]. Imaging of non-flowing microplastics and diatoms has been performed using holography with fibre-coupled solid state lasers [35]. Real-time in-flight monitoring has been demonstrated using extensive and complex laboratory-based optical apparatus such as fluorescence spectroscopy [36], while in-flight imaging of pollen grains has been carried out using holography with fluorescence spectroscopy [37], as well as using holography and an unmanned aerial vehicle (UAV) [38]. The ability to image and identify single pollen grains outdoors and in-flight using a small, simple device (e.g. Raspberry Pi microcomputer-size [39]) involving as few optics as possible would be invaluable for use in large-scale air-quality monitoring networks [40].

The spatial intensity distribution of the light scattered from a particulate varies depending on its chemical composition [41], and encodes information regarding the particulate's size, shape, structure and refractive index [42–45]. Identification of pollen grains directly from their scattering patterns has the potential to reduce the number of optics in a system, as an imaging lens would not be needed. Owing to the complexity of scattering patterns they typically cannot be categorised analytically, however, deep learning convolutional neural networks

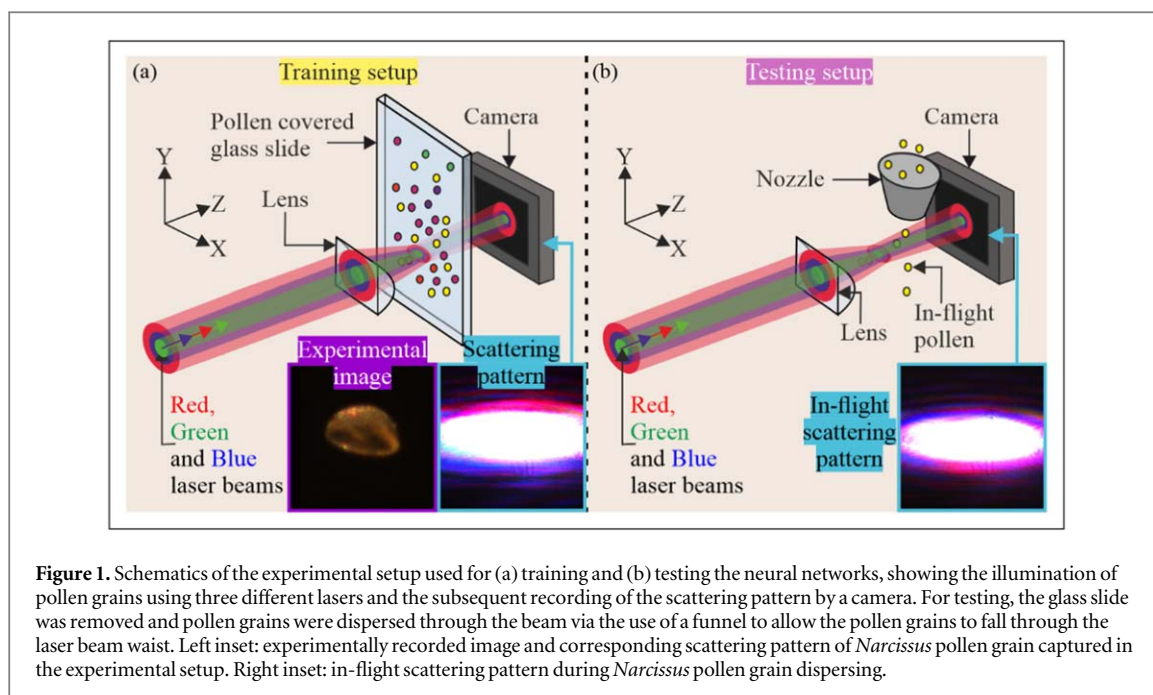


Figure 1. Schematics of the experimental setup used for (a) training and (b) testing the neural networks, showing the illumination of pollen grains using three different lasers and the subsequent recording of the scattering pattern by a camera. For testing, the glass slide was removed and pollen grains were dispersed through the beam via the use of a funnel to allow the pollen grains to fall through the laser beam waist. Left inset: experimentally recorded image and corresponding scattering pattern of *Narcissus* pollen grain captured in the experimental setup. Right inset: in-flight scattering pattern during *Narcissus* pollen grain dispersing.

[46–48] (such as those used to classify objects from images [49–52]) have been successfully employed to classify particulates such as pollen grains from their scattering patterns [53, 54]. Whilst previous work has also shown the ability to generate an image from the scattering pattern using deep learning [55], the particulates were mounted on a glass slide in one position in space, and were therefore stationary and not able to migrate in the manner typical for airborne pollen grains. Classification of airborne particulates is significantly more challenging because of the movement of the particulates (which necessitates shorter camera integration times) and also the fact that each particulate may not flow directly through the focus (and hence the neural network must have the capability to identify particulates at all positions throughout the focus). In this work, we simultaneously classify in-flight pollen grains from their scattering patterns, and generate images of those pollen grains directly from their scattering patterns.

Experimental methods

Sample fabrication

Pollen grains obtained from Sigma Aldrich, and the University of Southampton grounds, included *Populus deltoides* and *Narcissus*. All the pollen grains were deposited onto separate regions of a glass slide (borosilicate, 75 mm × 25 mm × 1 mm) to aid in the correct labelling and collection of scattering patterns.

Experimental setup

The experimental setup used to obtain scattering patterns for training and then testing the neural networks is shown in figure 1. Three collinear laser beams at central wavelengths of 450 nm, 520 nm and 635 nm, were focussed using a cylindrical lens (focal length of 15 cm) onto the surface of a glass slide. The resultant beam had a size at the focus of $\sim 100 \mu\text{m} \times 5 \text{ mm}$, with a confocal length of $\sim 10 \text{ mm}$. The pollen-covered glass slides were mounted on a motorized 3-axis stage (Zaber) that was automated using Python. The coordinate positions of the pollen grains on the slide were determined by imaging them using a camera (Thorlabs DCC1645C HQ, 1280 × 1024 pixels and a 50 × Olympus objective NA = 0.4). A white light source was employed to aid in the imaging and correct alignment of pollen grains. Subsequently, the imaging objective and white light source were removed and the camera sensor was placed 3 mm from the beam waist, along the laser axis, in order to collect scattering patterns from the pollen grains as they were translated in 3-dimensions (3D) through the beam. Afterwards, the pollen covered glass slide was removed and a 1 mm diameter nozzle was placed 5 mm above the beam, so that pollen grains could be dispersed under gravity through the beam and the scattering patterns of in-flight pollen grains recorded as a video sequence. The same camera settings (5 ms integration time) were used for recording the still images and the video recording.

Data collection

For each pollen grain (10 grains for each species), 1331 scattering pattern images were obtained, giving a total of 39930 scattering patterns for training the neural networks, which included images collected with the glass-slide removed, hence corresponding to a null category. For testing the neural networks on laser scattering patterns from in-flight pollen grains, *Populus deltoides* and then *Narcissus* pollen grains were dispersed through the nozzle and a video of the laser scatter was recorded. The scattering patterns and images of the pollen grains were cropped to 256×256 pixels, before being used as inputs for the neural networks.

Neural networks

Two neural networks were used in this work. Firstly, a convolutional neural network (CNN) based on Inception v3 [56] was used to categorise two different pollen grain species, as well as a null category, from their scattering patterns. Secondly, a conditional generative adversarial network (cGAN) [57] based on the network described in [58], was used to generate images of the pollen grains from their scattering patterns. The scattering pattern from an object depends on the intensity and phase of the electric field at that position. As the intensity and phase vary throughout a laser focus, the scattering pattern from an object is therefore dependent on the position of the object with respect to the laser focus. This poses a challenge when retrieving an image from a scattering pattern, as a single object may be associated with many scattering patterns. Here, we solve this challenge by training the neural network with additional positional data, namely the XYZ position of the object. The neural network is therefore trained to understand that differences in scattering patterns may correspond to the position of the object in addition to the size, shape and refractive index of the object. For convenience, we include this XYZ positional information as a red, green and blue (RGB) barcode in the pollen grain images, with different intensity levels corresponding to different positions in the 3D sensing volume. The generated images also included a 'barcode', which corresponded to the X, Y, and Z positions of the pollen grain(s), with respect to the laser focus, hence extending previous work achieved using pollen at a single position in space. As shown in figure 3, the barcode consisted of 3 lines of colour (RGB for XYZ in which the position was normalised to the range 0–255) inserted at the left of the target images for cGAN training, to be used as a 3D-space identifier. The motivation here was that the experimental scattering patterns would be dependent on the exact position of the pollen grain, particularly for the position through the focus along the axis of the laser path, and hence providing the pollen grain position during training would encourage the neural networks to understand the nature of the variation in scattering patterns. Note that the XYZ barcode was not needed for testing the neural network, and rather the neural network was trained to actually produce the barcode directly from each scattering pattern, i.e. to identify the XYZ position of the pollen grain from the scattering pattern. The neural networks were trained and tested on a computer using an NVIDIA RTX 2080 graphics processing unit (GPU). The time for training the image generation of the CNN was ~ 10 min, while the training for the cGAN was ~ 10 h. The processing time for generating each test image was ~ 6 milliseconds for the CNN and 130 milliseconds for the cGAN (including writing the generated image file to disc). Augmentation was used in the CNN training (random X and Y translation in the image of -5 and $+5$ pixels, with data in empty shifted regions set to zero, and using image scaling of 1 to $1.7\times$). The data was partitioned for training, validation and testing in the proportions 75:20:5, respectively. However, in the case of the species categorisation CNN, only 10% of the total data (10% of data from each grain, including equivalent amount for null category) were used, to reduce training times and allow faster iteration over the hyper-parameters. For the image reconstruction cGAN, 100% of the static training data was used, barring the same 201 scattering patterns that were also used for testing the CNN. Subsequently, 100 frames of video for each pollen species were used for testing the neural networks for in-flight predictions.

Results and discussion

The predictions of three different categories at different points within the 3D space of the laser beam waist are displayed as the confusion matrix shown in figure 3(a). The matrix shows the neural network correctly predicted 99% of the categories. Figures 3(b)–(d) show examples of experimental scattering patterns, experimental microscopy images, and images generated by the cGAN, for the case of (b) *Populus deltoides*, (c) *Narcissus* and (d) the null category.

To assist in understanding the capability of the CNN, figure 5(a) shows a cropped scattering pattern (for ease of highlighting regions) from the beam with no pollen present (null category), figure 5(b) displays a cropped version of the *Narcissus* scattering pattern from figure 4(c), and figure 5(c) shows the corresponding activation map (gradient-weighted class activation mapping technique [59]) of (b). The map shows the regions of the scattering pattern that were activated by the neural network during the classification decision (red strongest, blue weakest). This result indicates that the CNN was more strongly activated by the region of the beam where the

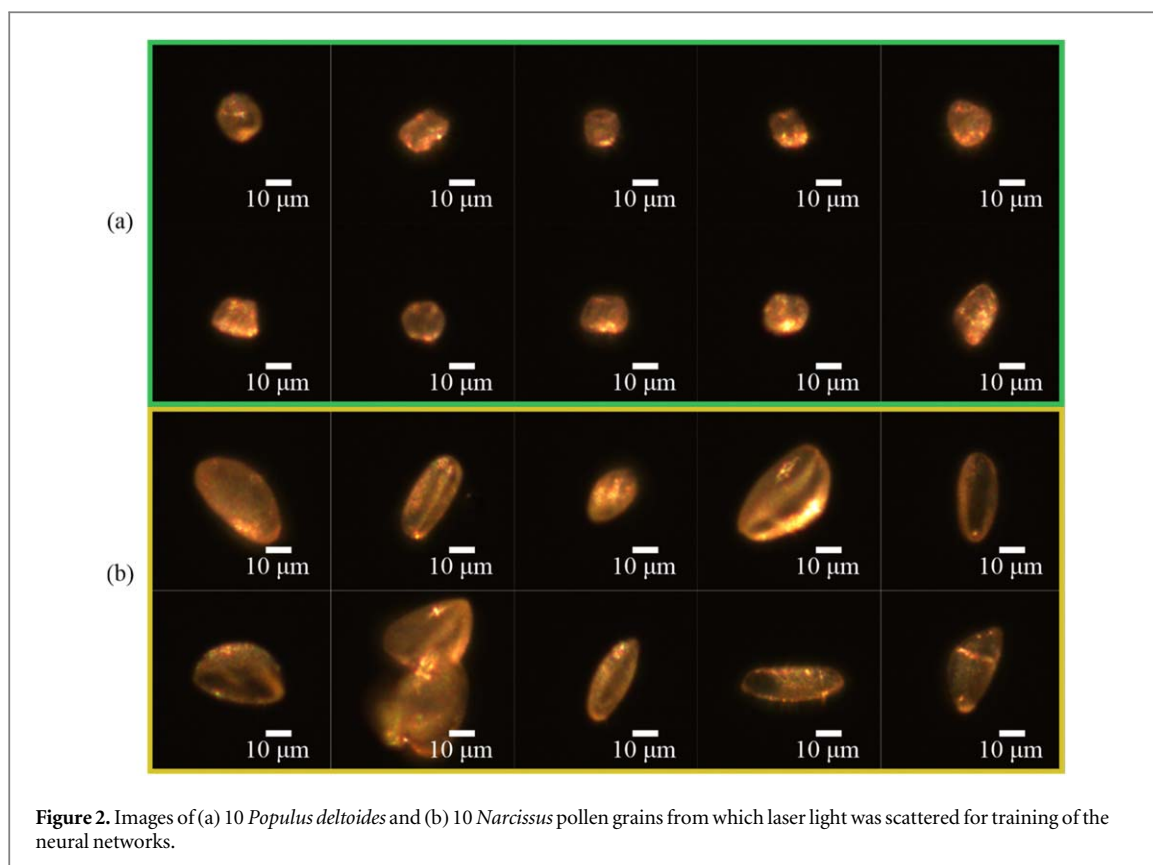


Figure 2. Images of (a) 10 *Populus deltoides* and (b) 10 *Narcissus* pollen grains from which laser light was scattered for training of the neural networks.

strongest scattering effects from the pollen grain were present. Both the activation and the accuracy of prediction by CNN gave confidence that the network could be used for sensing pollen grains in-flight.

Figure 6(a) shows classification results for 200 frames of video that were recorded during testing with airborne particles. Throughout the video, *Populus deltoides* (frames 1-100) and *Narcissus* (frames 101-200, via a funnel, into the laser beam focus) pollen grains, were dispersed through the laser beam. In addition, the frame-to-frame absolute change in the summed intensity of the image (normalised to 1) is also shown in the graph. Significant changes in intensity greater than the noise (~ 0.01 counts) are likely to indicate the presence of pollen and therefore allow us to identify frames where the null category was incorrectly assigned. For 100 frames of recording for *Populus deltoides* testing, 2 frames were identified as having pollen scattering patterns, while for 100 frames of recording for *Narcissus* testing, 6 frames were identified as having pollen grain scattering patterns. In total, out of the 200 frames, 37 had a significant change in intensity, with 8 of those having been detected by the neural network, while all the others were categorised as being null, meaning that $\sim 86\%$ of the frame predictions were correct.

Figure 6(b) shows predictions of the pollen grain appearance that were generated by the cGAN, from scattering patterns that were correctly classified by the CNN. The appearance of the pollen in the generated image of frame 126 shows similarity with the pollen grain type, namely *Narcissus*, albeit an image of a cluster of 3 pollen grains has been generated. An image generated from one of the correctly predicted null scattering patterns is also shown, as well as two images generated from correctly predicted *Populus deltoides* scattering patterns, although the pollen in frame 34 is very faint. The ability to reconstruct an image correctly is based on the input data used, hence features of the generated images are similar to those used in training. Moreover, errors in the predictions, both for pollen identification and imaging, could occur due to the possibility that although the species of pollen dispersed over the beam waist was known, these particulates could contain clusters of pollen grains in varying amounts. This could lead to incorrect categorisation of the pollen grains, as well as inability to reconstruct an image of the pollen (including the barcode) properly, since there was only one occurrence of a pollen grain cluster in the training data (see figure 2(b)).

In addition, the accuracy of prediction for airborne pollen was lower than in the case of the static (glass slide mounted) pollen, perhaps due to the potential effect of motion blur in the scattering patterns captured. It is estimated that the pollen could be travelling at 1 mms^{-1} at the laser focus due to gravity, meaning during an integration time of 5 ms, the pollen grain could have travelled $5 \mu\text{m}$, which is approximately $1/20^{\text{th}}$ of the beam waist). It may be possible to reduce the probability of incorrect categorisation of scattering patterns via the use of a more sensitive and faster camera sensor, as well as data augmentation, for example, training using

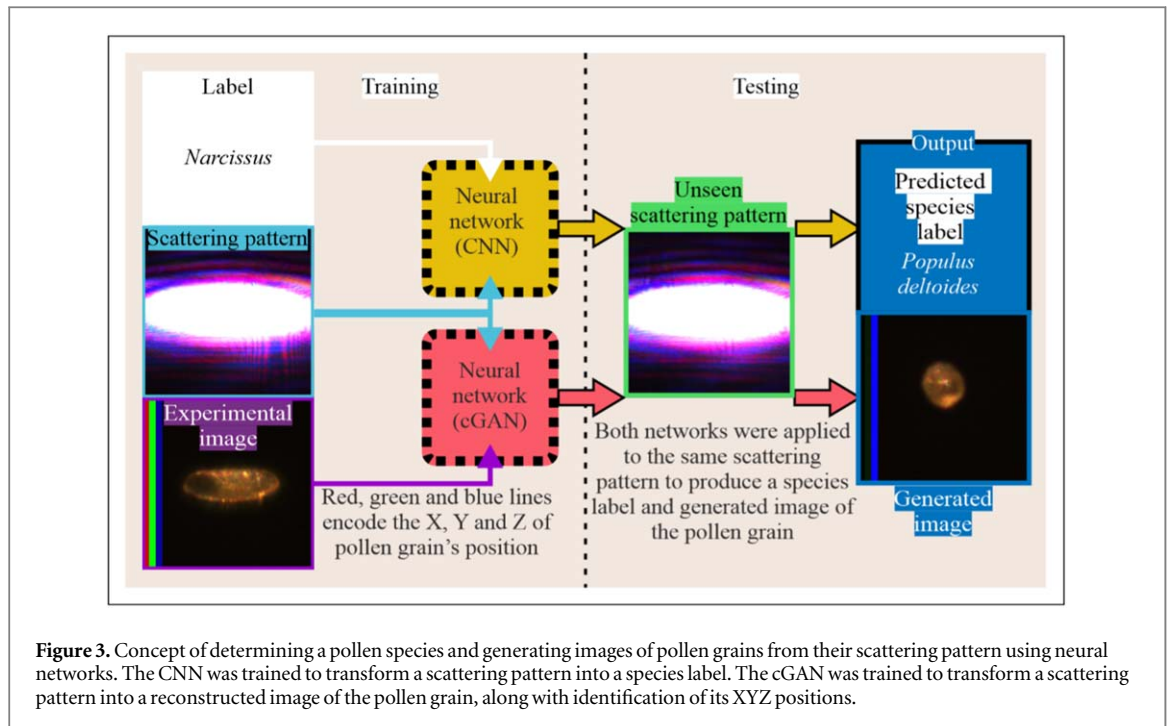


Figure 3. Concept of determining a pollen species and generating images of pollen grains from their scattering pattern using neural networks. The CNN was trained to transform a scattering pattern into a species label. The cGAN was trained to transform a scattering pattern into a reconstructed image of the pollen grain, along with identification of its XYZ positions.

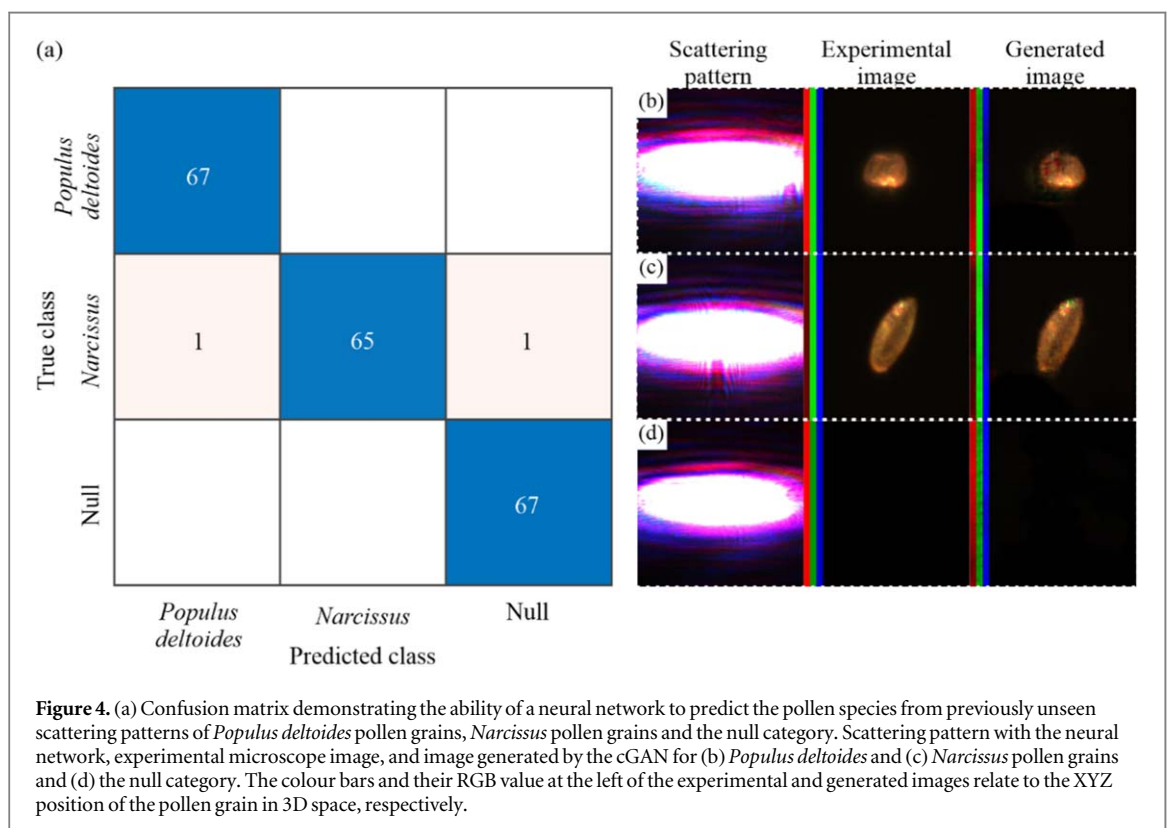


Figure 4. (a) Confusion matrix demonstrating the ability of a neural network to predict the pollen species from previously unseen scattering patterns of *Populus deltoides* pollen grains, *Narcissus* pollen grains and the null category. Scattering pattern with the neural network, experimental microscope image, and image generated by the cGAN for (b) *Populus deltoides* and (c) *Narcissus* pollen grains and (d) the null category. The colour bars and their RGB value at the left of the experimental and generated images relate to the XYZ position of the pollen grain in 3D space, respectively.

superposition of scattering patterns could help the neural network to identify species from clusters without significantly increasing training time [60]. Similarly, a larger amount of training data, via inclusion of more pollen grain clusters, could improve the neural network accuracy and image reconstruction (including the barcode specifying the pollen's XYZ position in space). With additional training data, one could identify many more species of pollen, via neural networks such as Inception v3, which is capable of categorising 1000s of different types of objects [56].

The mean wind speed in certain regions of the UK can be $\sim 3 \text{ ms}^{-1}$ [61], which is around 3 orders of magnitude greater than the particulate speeds used in this proof-of-principle demonstration. To adapt this

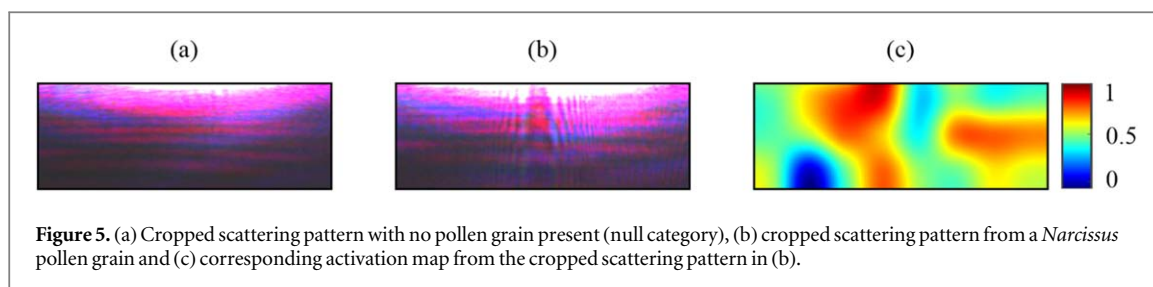


Figure 5. (a) Cropped scattering pattern with no pollen grain present (null category), (b) cropped scattering pattern from a *Narcissus* pollen grain and (c) corresponding activation map from the cropped scattering pattern in (b).

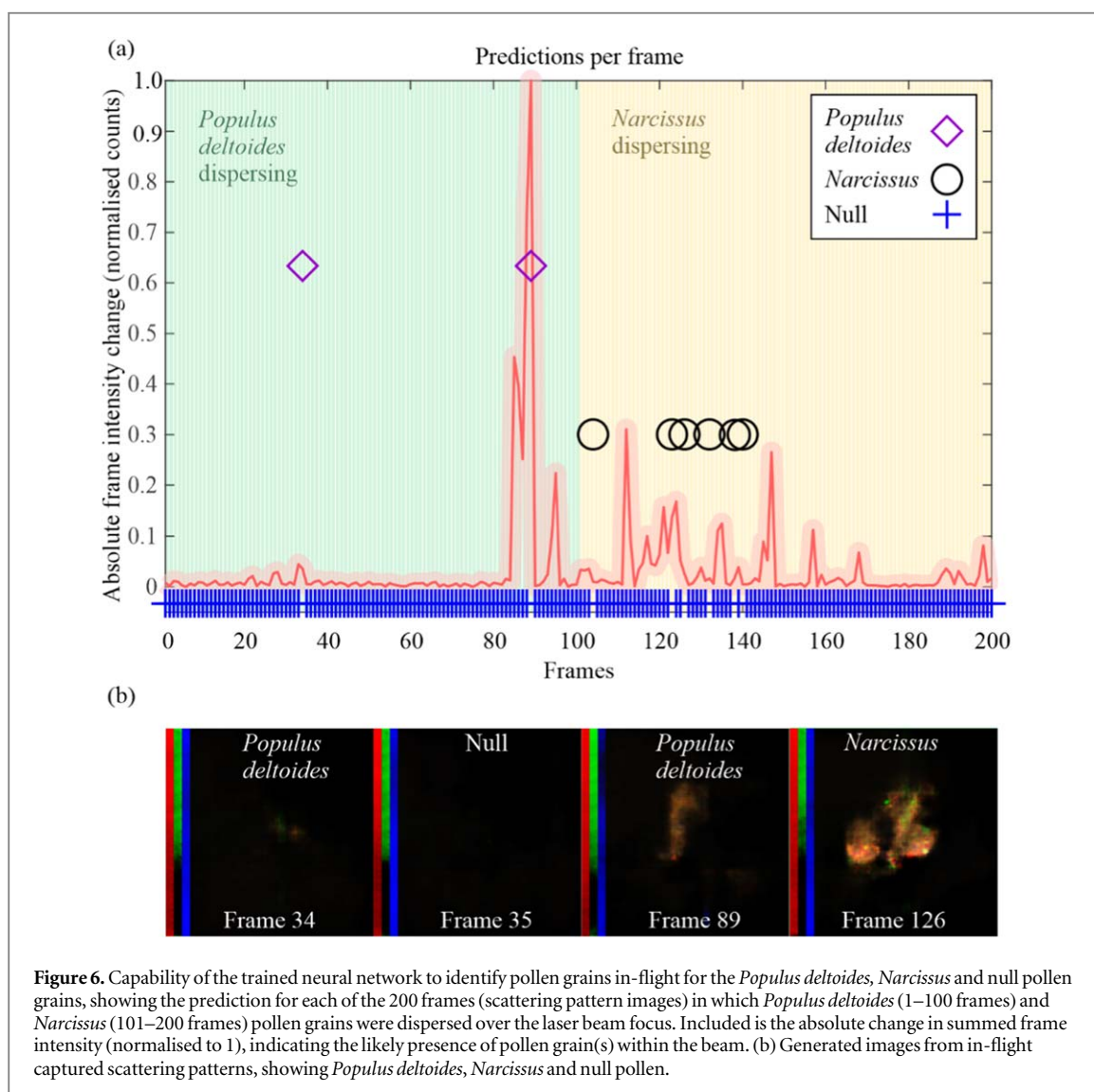


Figure 6. Capability of the trained neural network to identify pollen grains in-flight for the *Populus deltooides*, *Narcissus* and null pollen grains, showing the prediction for each of the 200 frames (scattering pattern images) in which *Populus deltooides* (1–100 frames) and *Narcissus* (101–200 frames) pollen grains were dispersed over the laser beam focus. Included is the absolute change in summed frame intensity (normalised to 1), indicating the likely presence of pollen grain(s) within the beam. (b) Generated images from in-flight captured scattering patterns, showing *Populus deltooides*, *Narcissus* and null pollen.

sensing technique for a typical outdoors environment where particulates may have higher speeds, one could use a sensor with a higher frame rate and gain, coupled with an increased laser power. In addition, air flow into the sensing volume near the camera sensor could be regulated using ducting, baffles and small fans as required [62, 63]. Finally, a 3D imaging setup could be created to allow real-time capture of the airborne particulates, allowing confirmation of the shape predictions generated by the cGAN, whilst simultaneously offering a rich source of additional training data.

Conclusion

To conclude, we have demonstrated the identification of pollen grains from their scattering patterns at different points in static 3D space (99% accuracy) and in-flight (~ 86% accuracy). We have also shown pollen grain image

generation in static 3D space and in-flight. Future work should consist of additional real-world measurements for a larger number of pollen species, which could include a category for unknown, since in the real-world there will likely be many scattering patterns recorded from untrained pollen grains and airborne particulates.

Acknowledgments

BM was supported by an EPSRC Early Career Fellowship (EP/N03368X/1) and EPSRC grant (EP/T026197/1).

Data availability statement

The data that support the findings of this study are openly available at the following URL/DOI:<https://doi.org/10.5258/SOTON/D1667>.

Conflicts of interest

The authors declare no conflict of interest.

ORCID iDs

James A Grant-Jacob  <https://orcid.org/0000-0002-4270-4247>

Matthew Praeger  <https://orcid.org/0000-0002-5814-6155>

Robert W Eason  <https://orcid.org/0000-0001-9704-2204>

Ben Mills  <https://orcid.org/0000-0002-1784-1012>

References

- [1] McInnes RN, Hemming D, Burgess P, Lyndsay D, Osborne NJ, Skjøth CA, Thomas S and Vardoulakis S 2017 Mapping allergenic pollen vegetation in UK to study environmental exposure and human health *Sci. Total Environ.* **599–600** 483–99
- [2] Rodinkova V V 2015 Airborne pollen spectrum and hay fever type prevalence in Vinnitsa, central Ukraine *Acta Agrobot.* **68** 383–9
- [3] Gruzieva O, Pershagen G, Wickman M, Melén E, Hallberg J, Bellander T and Löhmus M 2015 Exposure to grass pollen—but not birch pollen—affects lung function in Swedish children *Allergy* **70** 1181–3
- [4] Pawankar R, Canonica G W, Holgate ST, Lockey R F and Blaiss M S 2013 WAO white book on allergy: update 2013 *World Allergy Organ.* 11–9
- [5] Karatzas K, Katsifarakis N, Riga M, Werchan B, Werchan M, Berger U, Pfaar O and Bergmann K-C 2018 New European Academy of Allergy and Clinical Immunology definition on pollen season mirrors symptom load for grass and birch pollen-induced allergic rhinitis *Allergy* **73** 1851–9
- [6] Taketomi E A, Sopelete M C, de Sousa Moreira P F and de Assis Machado Vieira F 2006 Pollen allergic disease: pollens and its major allergens *Braz. J. Otorhinolaryngol.* **72** 562–7
- [7] Simoleit A, Wachter R, Gauger U, Werchan M, Werchan B, Zuberbier T and Bergmann K-C 2016 Pollen season of European beech (*Fagus sylvatica* L.) and temperature trends at two German monitoring sites over a more than 30-year period *Aerobiologia (Bologna)*. **32** 489–97
- [8] Caillaud D, Martin S, Segala C, Besancenot J-P, Clot B and Thibaudon M 2014 Effects of airborne birch pollen levels on clinical symptoms of seasonal allergic rhinoconjunctivitis *Int. Arch. Allergy Immunol.* **163** 43–50
- [9] Newnham R M, Sparks T H, Skjøth C A, Head K, Adams-Groom B and Smith M 2013 Pollen season and climate: Is the timing of birch pollen release in the UK approaching its limit? *Int. J. Biometeorol.* **57** 391–400
- [10] Buters J T M, Antunes C, Galveias A, Bergmann K C, Thibaudon M, Galán C, Schmidt-Weber C and Oteros J 2018 Pollen and spore monitoring in the world *Clin. Transl. Allergy* **8** 1–5
- [11] Corden J, Millington W, Bailey J, Brookes M, Caulton E, Emberlin J, Mullins J, Simpson C and Wood A 2000 UK Regional Variations in Betula Pollen (1993-1997) *Aerobiologia (Bologna)*. **16** 227–32
- [12] Galán C, Emberlin J, Domínguez E, Bryant R H and Villamandos F 1995 A Comparative analysis of daily variations in the gramineae pollen counts at Córdoba, Spain and London, UK *Grana* **34** 189–98
- [13] Emberlin J, Smith M, Rebecca C, Adams-Groom B and Beverly A G 2007 Changes in the pollen seasons of the early flowering trees *Alnus* spp. and *Corylus* spp. *International Journal of Biometeorology* **51** 181
- [14] Skypala I J, Calderon M A, Leeds A R, Emery P, Till S J and Durham S R 2011 Development and validation of a structured questionnaire for the diagnosis of oral allergy syndrome in subjects with seasonal allergic rhinitis during the UK birch pollen season *Clin. Exp. Allergy* **41** 1001–11
- [15] de Weger L A, Pashley C H, Šikoparija B, Skjøth C A, Kasprzyk I, Grewling Ł, Thibaudon M, Magyar D and Smith M 2016 The long distance transport of airborne Ambrosia pollen to the UK and the Netherlands from Central and south Europe *Int. J. Biometeorol.* **60** 1829–39
- [16] Suchan T, Talavera G, Sáez L, Ronikier M and Vila R 2019 Pollen metabarcoding as a tool for tracking long-distance insect migrations *Mol. Ecol. Resour.* **19** 149–62
- [17] Fernandez-Mensaque P C, Minero F J G, Morales J and Tomas C 1998 Forecasting olive (*Olea europaea*) crop production by monitoring airborne pollen *Aerobiologia (Bologna)*. **14** 185–90
- [18] Levetin E, Rogers C A and Hall S A 2000 Comparison of pollen sampling with a Burkard Spore Trap and a Tauber Trap in a warm temperate climate *Grana* **39** 294–302

- [19] Mari Bhat M and Rajasab A H 1989 Efficiency of vertical cylinder spore trap and seven day volumetric burkard spore trap in monitoring airborne pollen and fungal spores *Grana* **28** 147–153
- [20] Giesecke T, Fontana S L, Knaap W O, van der, Pardoe H S and Pidek I A 2010 *From early pollen trapping experiments to the Pollen Monitoring Programme Veg. Hist. Archaeobot.* **19** 247–58
- [21] Lagerstrom R, Holt K, Arzhaeva Y, Bischof L, Haberle S, Hopf F and Lovell D 2015 Pollen image classification using the Classifynder system: algorithm comparison and a case study on New Zealand honey *Adv. Exp. Med. Biol.* **823** 207–26
- [22] de Geus A R, Celia A Z B, Batista M A and da Silva S F 2019 *Large-scale Pollen Recognition with Deep Learning 2019 27th European Signal Processing Conference (EUSIPCO)* 1–5
- [23] Gallardo-Caballero R, García-Orellana C J, García-Manso A, González-Velasco H M, Tormo-Molina R and Macías-Macías M 2019 Precise pollen grain detection in bright field microscopy using deep learning techniques *Sensors* **19** 3583
- [24] Sevillano V and Aznarte J 2018 Improving classification of pollen grain images of the POLEN23E dataset through three different applications of deep learning convolutional neural networks *PLoS ONE* **13** e0201807
- [25] Sevillano V, Holt K and Aznarte J L 2020 Precise automatic classification of 46 different pollen types with convolutional neural networks *PLoS One* **15** e0229751
- [26] Gonçalves A B et al 2016 Feature Extraction and Machine Learning for the Classification of Brazilian Savannah Pollen Grains *PLoS ONE* **11** 1–20
- [27] Battiato S, Ortis A, Trenta F, Ascari L, Politi M and Siniscalco C 2020 *POLLEN13K: A Large Scale Microscope Pollen Grain Image Dataset 2020 IEEE International Conference on Image Processing (ICIP)* 2456–60
- [28] Huffman J A et al 2020 Real-time sensing of bioaerosols: Review and current perspectives *Aerosol Sci. Technol.* **54** 465–95
- [29] Schiele J, Rabe F, Schmitt M, Glaser M, Haring F, Brunner J O, Bauer B, Schuller B, Traidl-Hoffmann C and Damialis A 2019 Automated classification of airborne pollen using neural networks 2019 *41st Annual Int. Conf. of the IEEE Engineering in Medicine and Biology Society (EMBC)* 2019 4474–8
- [30] Oteros J, Pusch G, Weichenmeier I, Heimann U, Möller R, Röseler S, Traidl-Hoffmann C, Schmidt-Weber C and Buters J T M 2015 Automatic and online pollen monitoring *Int. Arch. Allergy Immunol.* **167** 158–66
- [31] Oteros J, Weber A, Kutzora S, Rojo J, Heinze S, Herr C, Gebauer R, Schmidt-Weber C B and Buters J T M 2020 An operational robotic pollen monitoring network based on automatic image recognition *Environ. Res.* **191** 110031
- [32] Kawashima S, Thibaudon M, Matsuda S, Fujita T, Lemonis N, Clot B and Oliver G 2017 Automated pollen monitoring system using laser optics for observing seasonal changes in the concentration of total airborne pollen *Aerobiologia (Bologna)*. **33** 351–62
- [33] Matsuda S and Kawashima S 2018 Relationship between laser light scattering and physical properties of airborne pollen *J. Aerosol Sci.* **124** 122–32
- [34] Mitsumoto K, Yabusaki K, Kobayashi K and Aoyagi H 2010 Development of a novel real-time pollen-sorting counter using species-specific pollen autofluorescence *Aerobiologia (Bologna)*. **26** 99–111
- [35] Bianco V, Memmolo P, Carcagni P, Merola F, Paturzo M, Distante C and Ferraro P 2020 Microplastic identification via holographic imaging and machine learning *Adv. Intell. Syst.* **2** 1900153
- [36] Šaulienė I et al 2019 Automatic pollen recognition with the Rapid-E particle counter: the first-level procedure, experience and next steps *Atmos. Meas. Tech.* **12** 3435–52
- [37] Sauvageat E, Zeder Y, Auderset K, Calpini B, Clot B, Crouzy B, Konzelmann T, Lieberherr G, Tummon F and Vasilatou K 2020 Real-time pollen monitoring using digital holography *Atmos. Meas. Tech.* **13** 1539–50
- [38] Kempainen O, Laning J C, Mersmann R D, Videen G and Berg M J 2020 Imaging atmospheric aerosol particles from a UAV with digital holography *Sci. Rep.* **10** 16085
- [39] Grant-Jacob J A, Xie Y, Mackay B S, Praeger M, McDonnell M D T, Heath D J, Loxham M, Eason R W and Mills B 2019 Particle and salinity sensing for the marine environment via deep learning using a Raspberry Pi *Environ. Res. Commun.* **1** 035001
- [40] Oteros J et al 2019 Building an automatic pollen monitoring network (ePIN): Selection of optimal sites by clustering pollen stations *Sci. Total Environ.* **688** 1263–74
- [41] Horvath H 1993 Atmospheric light absorption—A review *Atmos. Environ. Part A. Gen. Top.* **27** 293–317
- [42] Agrawal Y C, Whitmire A, Mikkelsen O A and Pottsmith H C 2008 Light scattering by random shaped particles and consequences on measuring suspended sediments by laser diffraction *J. Geophys. Res. Ocean.* **113**
- [43] Gibbs R J 1978 Light scattering from particles of different shapes *J. Geophys. Res. Ocean.* **83** 501–2
- [44] Bohren C F and Huffman D R 2008 *Absorption and Scattering of Light by Small Particles* (New York: Wiley)
- [45] Mills B et al 2008 Direct measurement of the complex refractive index in the extreme ultraviolet spectral region using diffraction from a nanosphere array *Appl. Phys. Lett.* **93** 231103
- [46] Szegedy C, Liu W, Jia Y, Sermanet P, Reed S, Anguelov D, Erhan D, Vanhoucke V and Rabinovich A 2015 Going deeper with convolutions *Proceedings of the IEEE conference on computer vision and pattern recognition* 1–9
- [47] LeCun Y, Bengio Y and Hinton G 2015 Deep learning *Nature* **521** 436
- [48] Serre T, Wolf L, Bileschi S, Riesenhuber M and Poggio T 2007 Robust object recognition with cortex-like mechanisms *IEEE Trans. Pattern Anal. Mach. Intell.* **411**–26
- [49] Krizhevsky A, Sutskever I and Hinton G E 2012 Imagenet classification with deep convolutional neural networks *Advances in Neural Information Processing Systems* **60** 1097–105
- [50] Simonyan K and Zisserman A 2014 Very deep convolutional networks for large-scale image recognition *arXiv Prepr. arXiv1409* 1556
- [51] Mollahosseini A, Chan D and Mahoor M H 2016 Going deeper in facial expression recognition using deep neural networks 2016 *IEEE winter conference on applications of computer vision (WACV)* 1–10
- [52] Ranjan R, Sankaranarayanan S, Bansal A, Bodla N, Chen J-C, Patel V M, Castillo C D and Chellappa R 2018 Deep learning for understanding faces: Machines may be just as good, or better, than humans *IEEE Signal Process Mag.* **35** 66–83
- [53] Grant-Jacob J A, Mackay B S, Baker J A G, Heath D J, Xie Y, Loxham M, Eason R W and Mills B 2018 Real-time particle pollution sensing using machine learning *Opt. Express* **26** 27237–46
- [54] Wu Y, Calis A, Luo Y, Chen C, Lutton M, Rivenon Y, Lin X, Koydemir H C, Zhang Y, Wang H et al 2019 Label-free Bio-aerosol Sensing Using On-Chip Holographic Microscopy and Deep Learning CLEO *Applications and Technology* **AM2K–AM23**
- [55] Grant-Jacob J A, Praeger M, Loxham M, Eason R and Mills B 2020 Lensless imaging of pollen grains at three-wavelengths using deep learning *Environ. Res. Commun.* (<https://doi.org/10.1088/2515-7620/aba6d1>)
- [56] Szegedy C, Vanhoucke V, Ioffe S, Shlens J and Wojna Z 2016 Rethinking the inception architecture for computer vision *Proceedings of the IEEE Conference on Computer Vision and Pattern Recognition* 2818–26
- [57] Isola P, Zhu J-Y, Zhou T and Efros A A 2017 Image-to-image translation with conditional adversarial networks *arXiv Prepr.* 5967–76

- [58] Grant-Jacob J A, Mackay B S, Baker J A G, Xie Y, Heath D J, Loxham M, Eason R W and Mills B 2019 A neural lens for super-resolution biological imaging *J. Phys. Commun.* (<https://doi.org/10.1088/2399-6528/ab267d>)
- [59] Selvaraju R R, Cogswell M, Das A, Vedantam R, Parikh D and Batra D 2020 Grad-CAM: visual explanations from deep networks via gradient-based localization *Int. J. Comput. Vis.* **128** 336–59
- [60] Perez L and Wang J 2017 The effectiveness of data augmentation in image classification using deep learning *arXiv Prepr. arXiv1712.04621*
- [61] Acosta J L and Djokić S Ž 2010 Assessment of renewable wind resources in UK urban areas *MELECON 2010-2010 15th IEEE Mediterranean Electrotechnical Conference* 1439–44
- [62] Wang Y, Li J, Jing H, Zhang Q, Jiang J and Biswas P 2015 Laboratory evaluation and calibration of three low-cost particle sensors for particulate matter measurement *Aerosol Sci. Technol.* **49** 1063–77
- [63] Alfano B, Barretta L, Del Giudice A, De Vito S, Di Francia G, Esposito E, Formisano F, Massera E, Miglietta M L and Polichetti T 2020 A review of low-cost particulate matter sensors from the developers' perspectives *Sensors* **20** 6819